# Intrinsic dense twinning via release of native strain

**Xianqi Song**
Jilin University https://orcid.org/0000-0002-4758-5865
**Chang Liu**
Jilin University https://orcid.org/0000-0003-0824-1098
**Quan Li** ( liquan777@jlu.edu.cn )
Jilin University https://orcid.org/0000-0002-7724-1289
**Yanming Ma**
Jilin University https://orcid.org/0000-0003-3711-0011
**Changfeng Chen**
Department of Physics and Astronomy, University of Nevada

**Article**

**Keywords:**

**Posted Date:** August 2nd, 2022

**DOI:** https://doi.org/10.21203/rs.3.rs-1881818/v1

# Intrinsic dense twinning via release of native strain

Xianqi Song,[1] Chang Liu,[1,2] Quan Li,[1,2,*] Yanming Ma,[1,2,†] and Changfeng Chen[3,‡]

[1]*State Key Lab of Superhard Materials and International Center for Computational Method and Software, College of Physics, Jilin University, Changchun 130012, China*

[2]*International Center of Future Science, Jilin University, Changchun 130012, China*

[3]*Department of Physics and Astronomy, University of Nevada, Las Vegas, Nevada 89154, USA*

(Dated: July 21, 2022)

Icosahedral boron-rich solids exhibit outstanding mechanical properties, but the crystal structure of this prominent class of materials has long remained enigmatic. Here, we report on a surprising discovery of an unprecedented twinning induced structural stabilization that creates highly twinned crystal structures that are stabler than the prevailing single crystal structure comprising complex multi-atom structural units. This phenomenon is showcased via a symmetry guided optimization process that produces a series of increasingly twinned $B_4C$ structures with progressively lower energy below that of the single crystal, and this behavior also occurs in multiple other boron-rich solids. These findings unveil a distinct paradigm of defect (twinning) induced structural stabilizing mechanism that reduces energy via release of native strains built in the complex structural units of the single crystal, creating an exceptional category of materials that comprise multiple domains of intrinsic dense twinning in the crystal structures.

A fundamental problem in condensed matter physics is to determine stable crystal structure and elucidate the influence on structural stability by defects that are ubiquitously present, by nature or by design, in all materials. It is generally accepted that the stable structure of a crystal hosts a periodic bonding pattern satisfying one of 230 space group symmetries and that defects such as vacancies, dislocations or grain boundaries break bonding symmetries and raise crystal energy[1–3]. This long established paradigm is rooted in considerations of chemical bonding and crystal symmetry, and is broadly adopted as the basis for constructing structural prototypes and evaluating structure-property relations[4–7]. Exceptions, however, may arise in materials comprising multi-atom structural units with complex intra-unit and inter-unit bonding connection patterns that create intrinsic strains in the single crystal, thereby opening a path for defect mediated bonding adjustment to release the native strains and stabilize the structure. To demonstrate this scenario, we showcase a distinct group of boron-rich compounds for a systematic exploration and an in-depth elucidation.

The light-element boron-rich compounds $B_nX$ (X=C, N, O, etc.) possess low density and high strength that are favorable for wide applications[8–11]. The constituent atoms in these compounds have similar electronegativity values that facilitate formation of B-X covalent bonds, and multi-center boron bonds promote diverse bonding patterns[12], generating structural units containing a large number of atoms, which greatly increases the difficulty for crystal structure determination. Meanwhile, close atomic radii of the X and B atoms make it hard for experimental distinction of atomic occupation sites, hindering accurate structural characterization. Early studies introduced the rhombohedral prototype structure containing icosahedral cages[13], which has been adopted for a large family of compounds, such as $B_4C$, $B_{13}C_2$, $\alpha$-B, and $B_6X$ (X=N, O, Si, P, S)[14]. Later experimental and computational advances further identified that the stable structure of $B_4C$ comprises $B_{11}C_p$(CBC) icosahedral units with carbon atom substituting for boron on the polar site ($C_p$) instead of the equatorial site ($C_e$) of the $B_{12}$ unit while the displaced boron atom joins the original three-atom carbon segment to form a CBC chain in the crystal structure[15–18]. Employing various crystal structure search methods[19–22], several recent studies predicted nonrhombohedral structures of $\alpha$-B, $B_4C$, $B_6N$, and $B_6O$[23–26].

Grain boundaries are a common type of structural defects, among which coherent twin boundaries (TBs) are most stable because the favorable lattice matching at the boundary minimizes the energy cost of forming the defective TBs relative to the single crystal[27]. Crystal twinning further enriches structural diversity of boron-rich complex covalent bonding solids. Synthesized boron-rich solids are often densely twinned[28–33], and first-principles calculations show that twinning raises the system energy but may also strengthen the resulting crystal structure[26,34–40], which is similar to observations made in nanotwinned diamond and cubic boron nitride[41–44]. Despite extensive past studies, there is still a lack of understanding of the nature of TBs in boron-rich solids, especially the rich variety and complex hierarchy of their structural forms and the atomistic mechanisms that determine their relative stability.

In this work, we report on an intriguing crystal twinning induced structural stabilization mechanism that optimizes the relation of local bonding symmetry and global stacking symmetry in a broad class of icosahedral boron-rich solids, which host complex multi-atom cages and chains as the basic structural building units. Remarkably, a symmetry guided optimization procedure produces twinning structures with energies that are below that of the established single crystal and become progressively lower with rising defect (twinning) density. This behavior runs counter to the common wisdom that structural defects would raise the crystal energy.

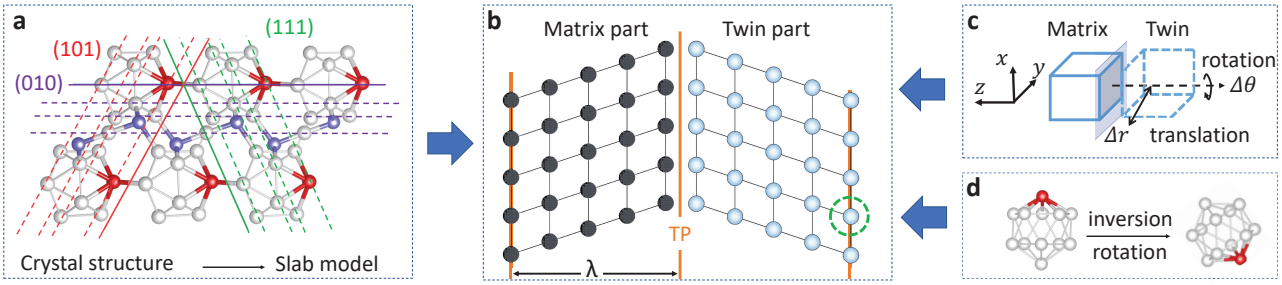


FIG. 1: **Construction of twinned crystal. a** A slab is cut from the single crystal to construct the matrix part of a TB structure. Here we use $B_4C$ as an exemplary material template, where boron atoms, carbon atoms on CBC chains and carbon atoms on icosahedra are represented by gray, lavender and red spheres, respectively. The solid lines indicate suitable cutting planes in the (101), (111), and (010) orientations for building the matrix part, while the parallel dotted lines in each orientation show improper cutting planes (more discussion on TP construction is given in Supplementary Information). **b** The twinning structure is formed by joining the matrix part and twin part at the twin plane, and the spacing between adjacent TPs is set by the thickness ($\lambda$) of the slab. **c** Splicing the matrix and twin part via selective translation or rotation of the twin part to achieve favorable bonding configurations at the TB. **d** Adjustment of local structure units (e.g., icosahedral $B_{11}C$ cage) via selective inversion or rotation for further optimization of the bonding connection at the TB.

Such unusual behaviors stem from a twinning-mediated release of native strains inherent in the complex bonding network, and this phenomenon is widely present in a variety of icosahedral boron-rich solids, such as $B_4C$, $B_6O$, $B_6N$, and $B_{13}CN$, that are conducive to hosting multiple energetically close densely twinned crystal domains. We further identified a broader variety of twinned boron-rich crystals that exhibit energies only slightly above that of the single crystal. These findings showcase a robust twinning-induced crystal stabilization mechanism among a prominent class of complex covalent bonding crystals, creating a new paradigm that enriches fundamental structure-stability relations for defects in crystalline solids.

## Results

**Principles and procedures in constructing twinned structure.** Here, we construct and evaluate TBs in a variety of boron-rich solids, focusing on the effect of bonding symmetry on the total energy. The procedure for constructing twinning structures is illustrated in Fig. 1 for the exemplary case of $B_4C$. The first step is to identify a suitable twin plane (TP) among various crystal orientations and cut a slab from the single crystal (Fig. 1a). A TB is then formed by joining a pair of matrix and twin parts that are in mutual mirror symmetry at a specific TP with adjustable slab thickness (Fig. 1b). Icosahedral boron-rich compounds contain complex, non-atom structural units, such as cages and chains, and different TP choices even with the same Miller index may lead to distinct TBs. To obtain optimal TP, it is imperative to find good bonding connections between the matrix and twin part via crystal matching operations, such as translational and rotational adjustments, as illustrated in Fig. 1c. Moreover, positional variations of the structural units with different bonding patterns (Fig. 1d) may also notably impact structural stability[39]. Since the TB dictated mirror symmetry alters the atomic positions and crystal orientations of the structural units from those of the single crystal, compatibility of the local structural-unit bonding symmetry with global TB stacking symmetry plays a crucial role in minimizing the twinning energy.

Following the procedure outlined above, we have constructed and examined a series of twinned $B_4C$ crystals based on the prevailing single-crystal structure $R$-$B_{11}C_p$(CBC). We find that bonding alignment at TP has a major impact on the relative stability of the resulting twinning structure. The twinned crystals with (111) and (101) oriented TPs (Supplementary Fig. 1) require substantial bonding adjustments across the TPs as outlined in Fig. 1c, d, including new bonding connections to avoid the energetically unfavorable intra-cage $C_e$ position and intercage $C_p$-$C_p$ bonds. Meanwhile, for the (010) oriented TP, TBs can be formed via orientational adjustments of the CBC chains and icosahedral cages to satisfy the mirror symmetry without the need to change any bonding connections inherited from the original single crystal. This preservation of bonding connectivity makes the (010)-twinned $B_4C$ energetically favorable.

**Structural stability of twinned $B_4C$ crystals.** Twinned crystals possess the characteristic symmetry with the lattice sites on the two sides of TPs forming mutual mirror images; but for multi-component materials, occupation of the lattice sites by different atomic species can lead to bonding configurations that do not strictly obey the mirror symmetry. In the case of $B_4C$, a (010) oriented twin model, referred to as Twin $A_n$ hereafter (Fig. 2a-c) was previously proposed. In this structure, the lattice sites obey the TP mirror symmetry before the structural relaxation caused by atomic (carbon) substitution in the otherwise all-boron $B_{12}$ icosahedral cage; however, the energetically dictated incorporation of the

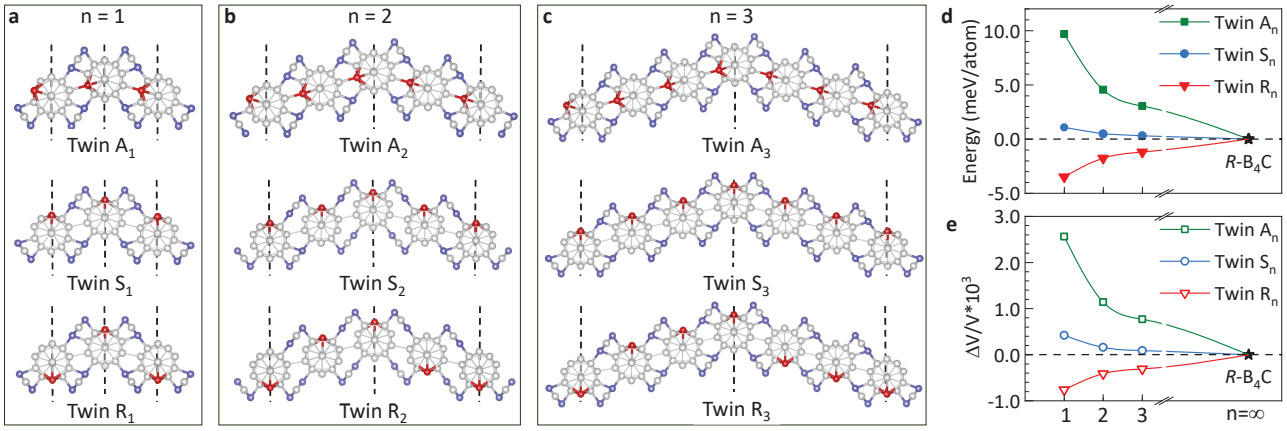


FIG. 2: **Structures and stability of twinned $B_4C$.** Three lowest-energy twinned crystals, Twin $A_n$, Twin $S_n$ and Twin $R_n$, with distinct (010) slab thicknesses marked by structure-unit index **a** $n$=1, **b** $n$=2, and **c** $n$=3. The incorporation of a carbon atom into each $B_{11}C$ cage causes a structural polarization as indicated by the directional alignment of the carbon atoms in the cages with respect to each other and to the TPs represented by vertical dashed lines (structural details are given in Supplementary Tables 1-3). **d**,**e** Energy and volume changes relative to the single crystal values, which are set to zero. In the $n \to \infty$ limit, all the twinned crystals tend to the prevailing single crystal rhombohedral $R$-$B_4C$ structure.

carbon atom generates distortion in the resulting $B_{11}C$ cage and breaks the structural symmetry at the atomic bonding level[15–18]. As a result, the bonding pattern in the twinned crystal becomes asymmetric about the TP (quantitative details are shown below); consequently, the resulting Twin A crystals no longer obey the mirror symmetry, thus violating the basic requirement for TBs. To remedy this problem, we have constructed two different (010) oriented twinned crystals by rotating the $B_{11}C$ cage to align the carbon atoms on the cages inside TPs to satisfy the full mirror symmetry of the structure units relative to the TP at the atomic bonding level. The resulting twinned crystals, referred to as Twin $S_n$ and Twin $R_n$, respectively, as also shown in Fig. 2a-c, exhibit detailed matching between the local (on-cage) bonding and TP mirror symmetry.

To assess the structure-stability relation of the low-energy twinned $B_4C$, we evaluate the energy variations with changing twinning density (Fig. 2d). Rising twinning density causes an obvious energy uptick in Twin $A_n$ structures; meanwhile, Twin $S_n$ series remain nearly degenerate with the single crystal even at the highest twinning density ($n$=1). Most remarkably, the energies of Twin $R_n$ structures become progressively lower than the single crystal as twinning density increases.

The sensitive microstructure dependent energy of twinned $B_4C$ showcases two major channels of strain release for structural optimization. The first channel is associated with the alignment of the carbon atom on the icosahedral cage that maximizes the local bonding symmetry with respect to the TP, thus minimizing the strains inside the cages. Specifically, the rotation of the $B_{11}C_p$ cage to align the carbon atoms on the TP optimizes the local bonding symmetry relative to the TP and lowers the energy via strain reduction inside the icosahedral cages, which is responsible for the significantly reduced energy of Twin $S_n$ versus Twin $A_n$. The second channel is related to the more subtle long-range strains built in the single crystal, which is reduced by breaking the translational symmetry via alternating structural (cage) polarization marked by the position of the carbon atom on the $B_{11}C_p$ cage, which further lowers the crystal energy of Twin $R_n$ and, surprisingly, brings the energy of the twinned $B_4C$ crystal below that of the single crystal.

## Discussion

**Bonding configurations of single and twinned $B_4C$ crystals.** To elucidate the microstructure-energy relation, we make a comparative study of the bonding structures of Twin $A_1$, Twin $S_1$ and Twin $R_1$ in comparison with the single crystal $R$-$B_4C$. The results (Fig. 3) show that the single crystal hosts an inhomogeneous distribution of bond lengths throughout the structural units. The average bond lengths on the two halves of the icosahedral $B_{11}C$ cage are notably different and so are the B-C bond lengths on the CBC chain, all of which indicate the presence of considerable native strains that cause bonding distortions in the crystal. Meanwhile, Twin $A_1$ possesses nearly identical bond-length disparities, reflecting similar amount and extent of native strains in the crystal, but the average bond lengths on the cage is slightly longer, leading to the higher energy compared to the single crystal. With the rotational adjustment aligning the on-cage carbon atoms inside the TPs, Twin $S_1$ hosts a more symmetric bonding arrangement relative to the TP, with identical average bond lengths on the two halves of each cage, but the results on cages in adjacent layers are different and the C-B bonds on the CBC chain also have different lengths, indicating reduced but residual strains in the crystal structure. Finally, after further adjusting the adjacent cages by alternating the alignments of the

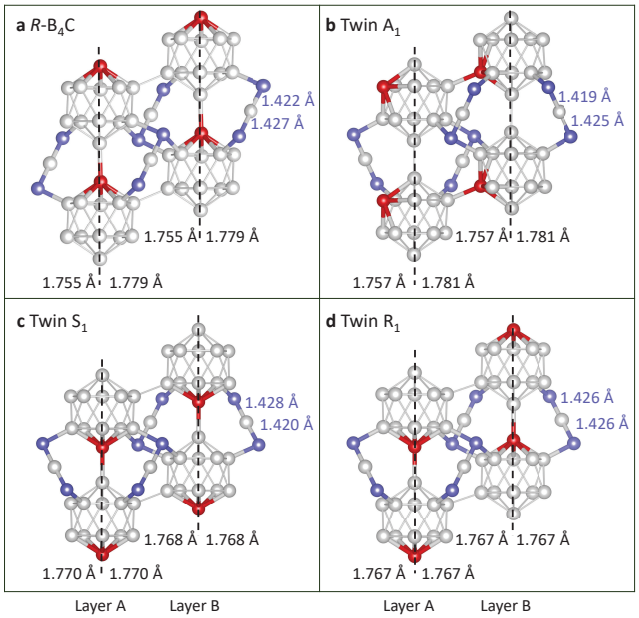


FIG. 3: **Bonding configurations of single and twinned $B_4C$ crystals.** **a** Single crystal $R$-$B_4C$. **b** Twin $A_1$. **c** Twin $S_1$. **d** Twin $R_1$. Listed are the average bond lengths on the left and right halves of the $B_{11}C$ cages in the two distinct primary stacking layers and those on the adjacent CBC chain in each case (details on bond-length data are given in Supplementary Table 4). The vertical dashed lines represent the (010) plane in the single crystal and TPs in the twinned crystal structures.

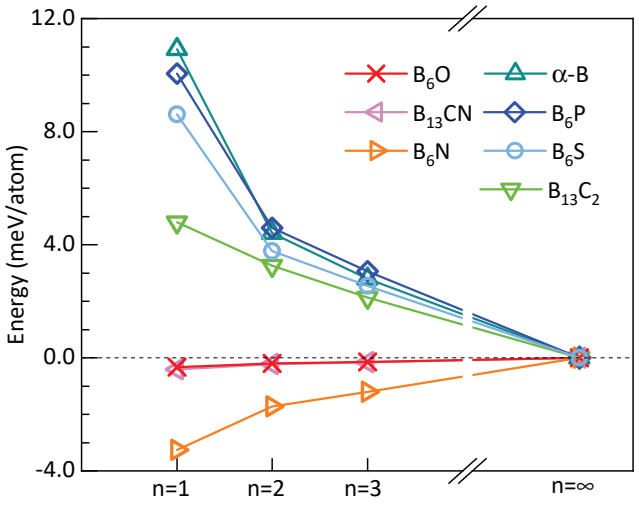


FIG. 4: **Stability of several representative twinned boron-rich solids.** Calculated energies of the twinning structures measured relative to the respective single-crystal results versus slab thickness index $n$ for indicated select boron-rich solids.

carbon-atom dictated structural polarization of the cages in neighboring slabs, Twin $R_1$ exhibits fully symmetric bonding arrangements with identical average bond lengths on the two halves of every cage and the same C-B bond lengths on the CBC chain throughout the crystal, indicating the effective removal of native strains originally built in the single crystal. This symmetry guided strain release creates a fully relaxed crystal with energy lower than the single crystal. The intrinsic strain states of various crystal structures are reflected in their volume change (Fig. 2e), which correlates perfectly with the energy (Fig. 2d), showing the strain effect on structural relaxation. This analysis highlights the mechanisms for energetic optimization by TB bonding adjustments.

Releasing strain energy via paired structural defects with contrasting topological features is known to occur in diverse physical systems, such as paired dislocations with opposite chirality or handedness in solids and liquid crystals[45–47] or vortex-antivortex pairs in magnets and superconductors[48–52]. These phenomena share the overarching mechanism in that distortions caused by individual defects are effectively compensated by the properly paired defects, thereby reducing the overall disturbance to the system thus lowering the energy cost. The $R$-$B_4C$ crystal hosts an intrinsic microstructural polarization due to the carbon atom incorporation into the boron icosahedron, which produces bonding distortions and the resulting native strains. The alternating stacking pattern with opposite polarization in neighboring matrix and twin parts of Twin $R_n$ crystal alleviates the long-range strain, leading to steadily decreasing energy below the single-crystal value with rising twin density. This finding expands the long-established optimally paired-defect stabilization paradigm to include TB induced strain release, which produces remarkable energetic optimization that is better than the original defect-free system, greatly enriching this prominent class of physical phenomena.

**Structure and stability of several twinned boron-rich solids.** To evaluate twinning stabilization of crystal structure as a broader phenomenon, we further examined a range of boron-rich solids and identified cases of twinning structures that are stabler than their respective prevailing single crystals (Fig. 4). A twinned $B_{13}CN$ structure (see Supplementary Fig. 2 for a snapshot) is lower in energy than single crystal $R$-$B_{13}CN$[53] driven by a rotation-inversion chain configuration at the TB that is effective in releasing the intrinsic strain energy built in the single crystal. Additional cases involve $R$-$B_6N$ and $R$-$B_6O$ (see Supplementary Fig. 2 for snapshots). Here, both N and O atoms have smaller atomic radii than B atom and the strong covalent B-N and B-O bonds tighten the distance between the neighboring cages, generating native strains in the single crystal. Twinning modifies the orientation of the B-N and B-O bonds to release the intrinsic strains, thereby lowering the energy to below the single-crystal values.

We also constructed twinning structures of $B_{13}C_2$, $\alpha$-B, $B_6P$, and $B_6S$ (see Supplementary Fig. 2 for structural snapshots), which exhibit slightly higher

but competitive energies compared to their respective single crystals (Fig. 4). Several factors prevent deeper twinning induced energy reduction here. For $B_{13}C_2$, the BCB chains do not support the rotation-inversion mechanism seen in $B_{13}CN$; meanwhile, $B_6P$ and $B_6S$ host large inter-cage distances due to the large atomic radii of P and S atoms and $\alpha$-B comprises multicenter bonding configurations[12], all of which do not promote twinning induced strain release. Nevertheless, the close energetic relations indicate that these boron-rich solids also favor multi-domain twinning structures that coexist with the single crystal phase.

In summary, we have developed a method for systematic construction and evaluation of stable twinning structures in complex covalent crystals via selection of energetically favorable twin-boundary orientation and stacking pattern combined with optimization of bonding symmetry of multi-atom structural units relative to the twin plane. This method has led to the surprising discovery of intrinsically densely twinned structures among icosahedral boron-rich solids, including $B_4C$, $B_{13}CN$, $B_6O$, and $B_6N$, which are stabler than their respective prevailing single crystals. This discovery establishes a distinct paradigm of defect (twinning) induced stabilization of crystals comprising complex structural units, resulting in multiple domains with variable twinning densities that coexist with the single crystal phase.

It is interesting to note that experimental techniques commonly used to reduce defect density and purify single crystal structure, such as thermal annealing, would have the opposite effect here by enhancing the density of twinning phases that have lower energy than the single crystal phase; consequently, pure phase single crystal structures are necessarily unattainable in this class of materials. Instead, specimens obtained under variable synthesis conditions may comprise different degrees of mixture of distinct twinning structures that are energetically close to each other. It is possible that other energetically competitive twinning patterns also appear in some cases. These extraordinary material behaviors expand the textbook description of the effect of twinning on crystal stability and define a distinct category of intrinsically twinned materials. These results enrich the knowledge and understanding of twinning in crystalline solids and provide a unique platform to explore the structure-property relations stemming from the newly identified native microstructural features, which may offer insights into distinct mechanisms governing deformation modes and stress responses that dominate structural evolution and dictate mechanical properties, opening unique paths for rational performance tuning and optimization.

## Methods

**First-principles calculations.** The first-principles total-energy calculations are carried out using local density approximation exchange correlation potential[54,55] as implemented in the Vienna *Ab initio* Simulation Package[56], adopting the projector augmented wave approach[57] to describe electron-ion interaction with $2s^22p^1$ and $2s^22p^2$ valence electron configurations for boron and carbon atoms, respectively. The plane wave basis set is constructed with an energy cutoff of 600 eV and the Brillouin zone is sampled under the Monkhorst-Pack scheme[58] with a $k$-point resolution of 2 $\pi$ $\times$0.03 Å$^{-1}$, achieving an energy convergence around 1 meV per atom.

**Construction of twinned $B_4C$ crystal.** A twinned $B_4C$ crystal is constructed by cutting a slab from its single crystal along a selected crystal plane, which serves as the twin plane (TP), then placing the mirror image of the slab across the TP to form the twinned structure. There are, however, constraints imposed by symmetry and energy that guide the choice of the most proper TPs. For example, the $(1\bar{1}0)$ plane is a mirror-symmetry plane of single-crystal $B_4C$ and thus cannot serve as a TP since the construction simply reproduces the original single crystal. On the other hand, the (111) plane can serve as a TP, but relative displacements are needed to match the matrix and twin part, as illustrated in Supplementary Fig. 1a. Here, the TPs are the vertical bisectors of the CBC chain with the $B_{11}C$ cages located on both sides of the TPs. Further adjustments of carbon-atom positions are made to avoid the high-energy intra-cage $C_e$ atoms and inter-cage $C_p$-$C_p$ bonds. Meanwhile, the (101) plane that goes through the center B atom on the CBC chain does not bisect the atomic chain, making it an improper TP choice; but the (101) plane that separates adjacent icosahedra and CBC chains can serve as a proper TP, as illustrated in Supplementary Fig. 1b, where the equatorial-position planes or polar-position planes are not parallel to the TP. The structural adjustments relative to the single crystal introduced to achieve adequate bonding at the TP renders these twinned crystals to become less energetically favorable than the single crystal. The lowest energy twined crystal is built with the TPs aligned in the (010) orientation as described in the main text of the paper. Here, the TPs traverse the $B_{11}$ cages and divide them into equal halves without altering the CBC chains or breaking and rearranging bonds across the TPs, resulting in the most energetically favorable twinned $B_4C$ crystal structure.

## Data availability

The authors declare that the main data supporting the findings of this study are available within the article and its Supplementary Information file.

* Electronic address: liquan777@jlu.edu.cn
† Electronic address: mym@jlu.edu.cn
‡ Electronic address: changfeng.chen@unlv.edu

## References


[1] Huang, Q. S. et al. Twinning-assisted dynamic adjustment of grain boundary mobility. *Nat. Commun.* **12**, 6695 (2021).

[2] Jin, H. X. et al. Atomistic mechanism of phase transformation between topologically close-packed complex intermetallics. *Nat. Commun.* **13**, 2487 (2022).

[3] Wang, Z. W. et al. High stress twinning in a compositionally complex steel of very high stacking fault energy. *Nat. Commun.* **13**, 3598 (2022).

[4] Kittle, C. *Introduction to Solid State Physics (8th ed.)* (Wiley, New York, 2005).

[5] Ashcroft, N. W. & Mermin, N. D. *Solid State Physics* (Saunders College Publishing, New York, 1976).

[6] Wang, Y. C. et al. Pressure-stabilized divalent ozonide $CaO_3$ and its impact on Earth's oxygen cycles. *Nat. Commun.* **11**, 4702 (2020).

[7] Peng, F. et al. Xenon iron oxides predicted as potential Xe hosts in Earth's lower mantle. *Nat. Commun.* **11**, 5227 (2020).

[8] Domnich, V., Reynaud, S., Haber, R. A. & Chhowalla, M. Boron carbide: structure, properties, and stability under stress. *J. Am. Ceram. Soc.* **94**, 3605-3628 (2011).

[9] Shirai, K. Electronic structures and mechanical properties of boron and boron-rich crystals (Part I). *J. Superhard Mater.* **32**, 205-225 (2010).

[10] Shirai, K. Electronic structures and mechanical properties of boron and boron-rich crystals (Part II). *J. Superhard Mater.* **32**, 336-345 (2010).

[11] Hubertet, H. et al. Icosahedral packing of $B_{12}$ icosahedra in boron suboxide ($B_6O$). *Nature* **391**, 376-378 (1998).

[12] Albert, B. & Hillebrecht, H. Boron: elementary challenge for experimenters and theoreticians. *Angew. Chem. Int. Ed.* **48**, 8640-8668 (2009).

[13] Clark, H. K. & Hoard, J. L. The crystal structure of boron carbide. *J. Am. Chem. Soc.* **65**, 2115-2119 (1943).

[14] David, E. Icosahedral boron-rich solids. *Phys. Today* **40**, 55-62 (1987).

[15] Kwei, G. H. & Morosin, B. Structures of the boron-rich boron carbides from neutron powder diffraction: implications for the nature of the inter-icosahedral chains. *J. Phys. Chem.* **100**, 8031-8039 (1996).

[16] Lazzari, R., Vast, N., Besson, J. M., Baroni, S. & Corso, A. D. Atomic structure and vibrational properties of icosahedral $B_4C$ boron carbide. *Phys. Rev. Lett.* **83**, 3230-3233 (1999).

[17] Vast, N., Besson, J. M., Baroni, S. & Corso, A. D. Atomic structure and vibrational properties of icosahedral $\alpha$-boron and $B_4C$ boron carbide. *Comput. Mater. Sci.* **17**, 127-132 (2000).

[18] Mauri, F., Vast, N. & Pickard, C. J. Atomic structure of icosahedral $B_4C$ boron carbide from a first principles analysis of NMR spectra. *Phys. Rev. Lett.* **87**, 085506 (2001).

[19] Oganov, A. R. & Glass, C. W. Crystal structure prediction using *ab initio* evolutionary techniques: Principles and applications. *J. Chem. Phys.* **124**, 244704 (2006).

[20] Pickard, C. J. & Needs, R. J. High-pressure phases of silane. *Phys. Rev. Lett.* **97**, 045504 (2006).

[21] Wang, Y. C., Lv, J., Zhu, L. & Ma, Y. M. Crystal structure prediction via particle swarm optimization. *Phys. Rev. B* **82**, 094116 (2010).

[22] Wang, Y. C., Lv, J., Zhu, L. & Ma, Y. M. CALYPSO: a method for crystal structure prediction. *Comput. Phys. Commun.* **183**, 2063-2070 (2012).

[23] Pickard, C. J. & Needs, R. J. *Ab initio* random structure searching. *J. Phys.: Condens. Matter* **23**, 053201 (2011).

[24] An, Q. Prediction of superstrong $\tau$-boron carbide phase from quantum mechanics. *Phys. Rev. B* **95**, 100101 (2017).

[25] Wang, L. Y. et al. Novel superhard boron-rich nitrides under pressure. *Sci. China Mater.* **63**, 2358-2364 (2020).

[26] An, Q. et al. Nanotwinned boron suboxide ($B_6O$): New ground state of $B_6O$. *Nano Lett.* **16**, 4236-4242 (2016).

[27] Lu, K. Stabilizing nanostructures in metals using grain and twin boundary architectures. *Nat. Rev. Mater.* **1**, 1 (2016).

[28] Heian, E. M. et al. High-defect-concentration $B_4C$ through mechanical activation and field-assisted combustion. *J. Am. Ceram. Soc.* **87**, 779-783 (2004).

[29] Anselmi-Tamburiniw, U., Munir, Z. A., Kodera, Y., Imai, T. & Ohyanagi, M. Influence of synthesis temperature on the defect structure of boron carbide: experimental and modeling studies. *J. Am. Ceram. Soc.* **88**, 1382-1387 (2005).

[30] Chang, B., Gersten, B. L., Szewczyk, S. T. & Adams, J. W. Characterization of boron carbide nanoparticles prepared by a solid state thermal reaction. *Appl. Phys. A* **86**, 83-87 (2007).

[31] Suri, A. K., Subramanian, C., Sonber, J. K. & Ch Murthy, T. S. R. Synthesis and consolidation of boron carbide: a review. *Int. Mater. Rev.* **55**, 4-40 (2010).

[32] Xie, K. Y., Kuwelkar, K., Haber, R. A., LaSalvia, J. C. & Hemker, K. J. Microstructural characterization of a commercial hot-pressed boron carbide armor plate. *J. Am. Ceram. Soc.* **99**, 2834-2841 (2016).

[33] Toksoy, M. F. et al. Densification and characterization of rapid carbothermal synthesized boron carbide. *Int. J. Appl. Ceram. Technol.* **14**, 443-453 (2017).

[34] An, Q. & Goddard III, W. A. Atomistic origin of brittle failure of boron carbide from large-scale reactive dynamics simulations: suggestions toward improved ductility. *Phys. Rev. Lett.* **115**, 105501 (2015).

[35] An, Q. Superstrength through nanotwinning. *Nano Lett.* **16**, 7573-7579 (2016).

[36] Yang, X. K., Coleman, S. P., Lasalvia, J. C., Goddard, W. A. & An, Q. Shear-induced brittle failure along grain boundaries in boron carbide. *ACS Appl. Mater. Interfaces* **10**, 5072-5080 (2018).

[37] An, Q., Reddy, K. M., Xie, K. Y., Hemker, K. J. & Goddard III, W. A. New ground-state crystal structure of elemental boron. *Phys. Rev. Lett.* **117**, 085501 (2016).

[38] Fujita, T. et al. Asymmetric twins in rhombohedral boron carbide. *Appl. Phys. Lett.* **104**, 021907 (2014).

[39] Xie, K. Y. et al. Atomic-level understanding of "asymmetric twins"in boron carbide. *Phys. Rev. Lett.* **115**, 175501 (2015).

[40] An, Q. et al. Nucleation of amorphous shear bands at nanotwins in boron suboxide. *Nat. Commun.* **7**, 11001 (2016).

[41] Tian, Y. J. et al. Ultrahard nanotwinned cubic boron nitride. *Nature* **493**, 385-388 (2013).

[42] Li, B., Sun, H. & Chen, C. F. Large indentation strain stiffening in nanotwinned cubic boron nitride. *Nat. Commun.* **5**, 4965 (2014).

[43] Huang, Q. et al. Nanotwinned diamond with unprecedented hardness and stability. *Nature* **510**, 250-253 (2014).

[44] Li, B., Sun, H. & Chen, C. F. Extreme mechanics of probing the ultimate strength of nanotwinned diamond. *Phys. Rev. Lett.* **117**, 116103 (2016).

[45] Kleman, M. & Friedel, J. Disclinations, dislocations, and continuous defects: a reappraisal. *Rev. Mod. Phys.* **80**, 61-115 (2008).

[46] Pieranski, P. Dislocations and other topological oddities. *C. R. Phys.* **17**, 242-263 (2016).

[47] Repula, A. & Grelet, E. Elementary edge and screw dislocations visualized at the lattice periodicity level in the smectic phase of colloidal rods. *Phys. Rev. Lett.* **121**, 097801 (2018).

[48] Geurts, R., Milošević, M. V. & Peeters, F. M. Symmetric and asymmetric vortex-antivortex molecules in a fourfold superconducting geometry. *Phys. Rev. Lett.* **97**, 137002 (2006).

[49] Neal, J. S. et al. Competing symmetries and broken bonds in superconducting vortex-antivortex molecular crystals. *Phys. Rev. Lett.* **99**, 127001 (2007).

[50] Iavarone, M. et al. Imaging the spontaneous formation of vortex-antivortex pairs in planar superconductor/ferromagnet hybrid structures. *Phys. Rev. B* **84**, 024506 (2011).

[51] Rybakov, F. N., Pervishko, A., Eriksson, O. & Babaev, E. Antichiral ferromagnetism. *Phys. Rev. B* **104**, L020406 (2021).

[52] Karna, S. K. et al. Annihilation and control of chiral domain walls with magnetic fields. *Nano Lett.* **21**, 1205-1212 (2021).

[53] Liang, H., Li, Q. & Chen, C. F. Atomistic mechanisms for contrasting stress-strain relations of $B_{13}CN$ and $B_{13}C_2$. *J. Phys. Chem. Lett.* **11**, 10454-10462 (2020).

[54] Ceperley, D. M. & Alder, B. J. Ground state of the electron gas by a stochastic method. *Phys. Rev. Lett.* **45**, 566-569 (1980).

[55] Perdew, J. P. & Zunger, A. Self-interaction correction to density-functional approximations for many-electron systems. *Phys. Rev. B* **23**, 5048-5079 (1981).

[56] Kresse, G. & Furthmüller, L. Efficient iterative schemes for *ab initio* total-energy calculations using a plane-wave basis set. *Phys. Rev. B* **54**, 11169-11186 (1996).

[57] Kresse, G. & Joubert, J. From ultrasoft pseudopotentials to the projector augmented-wave method. *Phys. Rev. B* **59**, 1758-1775 (1999).

[58] Monkhorst, H. J. & Pack, J. D. Special points for Brillouin-zone integrations. *Phys. Rev. B* **13**, 5188-5192 (1976).


## Acknowledgements

This research was supported by the National Key Research and Development Program of China (Grant Nos. 2018YFA0703400), Natural Science Foundation of China (Grant Nos. 12074140 and 12034009), the Fundamental Research Funds for the Central Universities (Jilin University, JLU), and Program for JLU Science and Technology Innovative Research Team (JLUSTIRT). Reported calculations utilized computing facilities at the High-Performance Computing Center of Jilin University.

## Author contributions

Q.L., Y.M., and C.C. designed research; X.S. and C.L. performed research; X.S., C.L., Q.L., Y.M., and C.C. analyzed data and wrote the paper.

X.S. and C.L. contributed equally to this work.

## Competing interests

The authors declare no competing interests.

## Additional information

**Supplementary information** The online version contains supplementary material available at

**Correspondence** and requests for materials should be addressed to Quan Li, Yanming Ma or Changfeng Chen.

# Supplementary Files

This is a list of supplementary files associated with this preprint. Click to download.

- SupplementaryInformationofB4C.docx